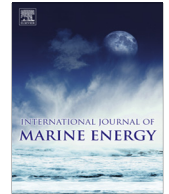




ELSEVIER

Contents lists available at ScienceDirect

## International Journal of Marine Energy

journal homepage: [www.elsevier.com/locate/ijome](http://www.elsevier.com/locate/ijome)

# Reactive control of a wave energy converter using artificial neural networks



E. Anderlini <sup>a,c,d,\*</sup>, D.I.M. Forehand <sup>b</sup>, E. Bannon <sup>c</sup>, M. Abusara <sup>d</sup>

<sup>a</sup> Industrial Doctoral Centre for Offshore Renewable Energy, University of Edinburgh, Faraday Building, Colin Maclaurin Road, Edinburgh EH9 3DW, UK

<sup>b</sup> Institute of Energy Systems, University of Edinburgh, Faraday Building, Colin Maclaurin Road, Edinburgh EH9 3DW, UK

<sup>c</sup> Wave Energy Scotland, 10 Inverness Campus, Inverness IV2 5NA, UK

<sup>d</sup> College of Engineering, Mathematics and Physical Sciences, University of Exeter, Penryn Campus, Penryn TR10 9FE, UK

## ARTICLE INFO

### Article history:

Received 23 March 2017

Accepted 7 August 2017

Available online 12 August 2017

### Keywords:

Wave Energy Converter (WEC)

Artificial Neural Networks (ANNs)

Reactive control

Multistart optimization

## ABSTRACT

A model-free algorithm is developed for the reactive control of a wave energy converter. Artificial neural networks are used to map the significant wave height, wave energy period, and the power take-off damping and stiffness coefficients to the mean absorbed power and maximum displacement. These values are computed during a time horizon spanning multiple wave cycles, with data being collected throughout the lifetime of the device so as to train the networks off-line every 20 time horizons. Initially, random values are selected for the controller coefficients to achieve sufficient exploration. Afterwards, a Multistart optimization is employed, which uses the neural networks within the cost function. The aim of the optimization is to maximise energy absorption, whilst limiting the displacement to prevent failures. Numerical simulations of a heaving point absorber are used to analyse the behaviour of the algorithm in regular and irregular waves. Once training has occurred, the algorithm presents a similar power absorption to state-of-the-art reactive control. Furthermore, not only does dispensing with the model of the point-absorber dynamics remove its associated inaccuracies, but it also enables the controller to adapt to variations in the machine response caused by ageing.

© 2017 The Authors. Published by Elsevier Ltd. This is an open access article under the CC BY license (<http://creativecommons.org/licenses/by/4.0/>).

## 1. Introduction

With a possible resource of up to 2.1 TW of power worldwide [1], wave energy can become an important future energy resource, thus decreasing society's greenhouse gas emissions. At the moment, the wave energy industry is not mature yet: numerous Wave Energy Converter (WEC) devices have been developed, but none has been established as the best design yet. Reference [2] provides a thorough review of some of the most promising recent technologies. Point absorbers are an established type of offshore WECs [2]. They comprise of a floating body, whose dimensions are small relative to the characteristic wavelength, excited by ocean waves that drive a power take-off (PTO) system, which absorbs energy. WECs are envisioned to be installed in groups, i.e. wave farms, so as to reap the benefits of economies of scale [3]. However, for simplicity we analyse a single, axisymmetric unit subject to motions in heave.

\* Corresponding author at: Industrial Doctoral Centre for Offshore Renewable Energy, University of Edinburgh, Faraday Building, Colin Maclaurin Road, Edinburgh EH9 3DW, UK.

E-mail address: [E.Anderlini@ed.ac.uk](mailto:E.Anderlini@ed.ac.uk) (E. Anderlini).

Over the years, various control schemes have been proposed for the maximization of energy absorption of WECs, with [4,5] presenting comprehensive reviews of the initial and recent studies in the field. In theory, optimal power generation can be obtained through complex-conjugate control, since it regulates the system so as to achieve resonance with the incoming waves [4]. Nevertheless, this is impractical in reality due to the associated large motions of, and loads on, the machine in extreme seas. Thus, alternative control strategies have been implemented, which consider physical constraints on the motions, forces and power rating of the WEC [3].

Latching, model-predictive and simple-but-effective control are real-time techniques for the control of WECs. With latching control, first developed by [6], there is an alternation over a wave cycle of stages when the device is linearly damped and locked in place by the PTO system. Resonance is achieved by regulating the duration of each phase [7]. Model predictive control computes at each time step the force that maximizes energy absorption during a future time horizon [8,9]. Simple-but-effective control applies a force that is calculated by fitting a narrow-banded function to the wave excitation force [10]. While the scaling of latching control to wave farms poses serious problems, [11] have applied model predictive control to multi-body WECs, and [12,13] to an array of three point absorbers. Although these methods include limits on the response and loading of WECs, their behaviour is strongly influenced by the quality of the forecast wave excitation force and of the model of the device dynamics [5]. In addition, model predictive control presents a very high computational cost associated with the real-time optimization. Simple-but-effective control results in similar power generation to model predictive control, but presents a simpler implementation [5].

An alternative type of control strategies relies on time-averaged sea states, thus assuming stationary wave conditions over a prescribed time [3]. With reactive control, simulations are run to calculate the combination of PTO damping and stiffness coefficients that maximise the generated energy in each sea state. Resistive control represents a specific case, where the stiffness term is zero. Force and displacement constraints can be included within the numerical model and cost function, respectively. While this technique may be associated with lower energy extraction than on-line control strategies [13], it is less computationally intensive and presents a simple implementation. Furthermore, the control scheme can be easily extended to the treatment of wave farms, as considered by [3].

All aforementioned methods are strongly affected by the accuracy of the model of the body dynamics they use. For this reason, modelling errors can result in a drop in the generated power. Additionally, the control strategies cannot adapt to changes in the response of the WEC caused by its ageing, with marine biofouling playing a major role. Therefore, in a previous article the authors have developed an algorithm for resistive control based on reinforcement learning that learns the optimal PTO damping coefficient in every sea state directly from experience [14]. This work has been extended to the reactive control of a point absorber in [15]. In contrast to resistive control, reactive control can lead to much higher efficiencies but requires an extension of the search space to two variables, namely the PTO damping and stiffness coefficients. For this reason, learning time in each sea state can become very long depending on the refinement of the discretization of the PTO coefficients. Furthermore, continuous values of the control parameters could result in higher efficiencies. Artificial Neural Networks (ANNs) represent an alternative set of machine learning algorithms which are popular in the computer science industry. They can yield smooth, non-linear function approximations [16] and therefore provide an elegant solution to the above two problems with reinforcement learning. ANNs have been used to provide real-time system identification for WEC dynamics by [17,18]. Furthermore, [17] have successfully applied the ANNs model to the control of the AWS Archimedes Swing WEC.

Here, ANNs will be applied for the first time to the reactive control of a point absorber. Hence, they are employed to map the sea state conditions averaged over a time interval and the applied PTO coefficients to the mean power and maximum displacement that occur over the duration of the time interval. The resulting mapping will be used to select optimal PTO damping and stiffness coefficient at the start of each time interval, once learning has been completed. Numerical simulations are run in both regular and irregular waves to test the efficiency and convergence properties of the proposed control algorithm.

## 2. Reactive control of a point absorber

### 2.1. System description

A point-absorber with an electromechanical PTO is considered, as for example analysed by [19] or proposed by [20]. Removing the hydraulic stage in the power conversion process results in an increase in efficiency [20]. Furthermore, as opposed to direct-drive PTO, the use of smaller, cheaper rotating generators is still possible [20].

As shown in Fig. 1, the movement of the float is converted into rotational motion through a mechanical stage. This mechanism drives a generator, which can be of a permanent magnet design as proposed by [20]. A variable-frequency converter delivers the generated power to the electrical grid at the requested frequency. The controller controls the generator through the machine-side converter in order to maximise energy absorption. The grid-side converter keeps a constant DC-link voltage and controls the active and reactive power transmitted to the network [21].

In order to select optimal control actions, the controller requires the heaving body displacement,  $z$ , and velocity,  $\dot{z}$ , as well as the wave elevation,  $\zeta$ . While the former two variables are inferred from on-board accelerometers, the latter is usually provided by an separate wave buoy for the whole wave farm. Furthermore, the generated power  $P$  is obtained from the electric PTO system.

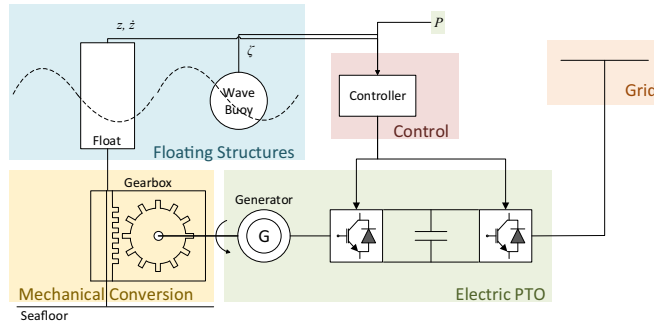


Fig. 1. Schematic diagram of the WEC with its electromechanical PTO.

2.2. Hydrodynamics modelling

The hydrodynamic model has been obtained as in [14]. With the assumptions of small body motions and linear wave theory, it is possible to express the response of the point absorber through the superposition of inertial, hydrostatic, radiation, excitation and control forces [22]. Therefore, modelling the radiation force according to Cummins [23], it is possible to obtain the following time-domain equation of motion of the WEC [24]:

$$(M + A_{3,3}(\infty))\ddot{z}(t) + \int_0^t K_{3,3}(t - \tau)\dot{z}(\tau)d\tau + C_{3,3}z(t) = F_3(t) + F_{PTO}(t), \tag{1}$$

with the index 3 expressing heaving motions.  $M$  is the float mass,  $C_{3,3}$  the hydrostatic stiffness coefficient,  $A_{3,3}(\infty)$  the added mass at infinite wave frequency, and  $K_{3,3}(t)$  the radiation impulse response function. The panel-code WAMIT has been used for their determination. The right-hand side of (1) comprises of the sum of the PTO force,  $F_{PTO}$ , and the wave excitation force,  $F_3$ . The derivation of (1), as well as a more thorough explanation can be found in [25].

Eq. (1) is shown graphically in Fig. 2. The radiation force is approximated through a state-space system in order to speed up the simulations. The state-space matrices have been computed as described in [24].

2.3. Reactive control

As can be seen in Fig. 2, with reactive control the sum of a damping and a stiffness term yields the PTO force [3]:

$$F_{PTO}(t) = B_{PTO}\dot{z}(t) + C_{PTO}z(t). \tag{2}$$

In electromechanical PTO units, variations in the generator excitation current or the power converter conduction angle result in changes in the PTO damping and stiffness coefficients [5],  $B_{PTO}$  and  $C_{PTO}$  respectively. As we deal with  $B_{PTO}$  and  $C_{PTO}$  directly in this article for simplicity, the method may in fact be applied to hydraulic or direct-drive PTO systems as well.

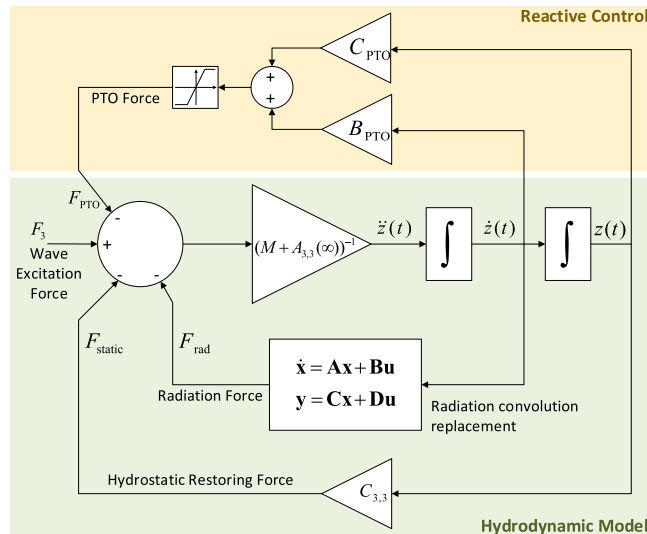
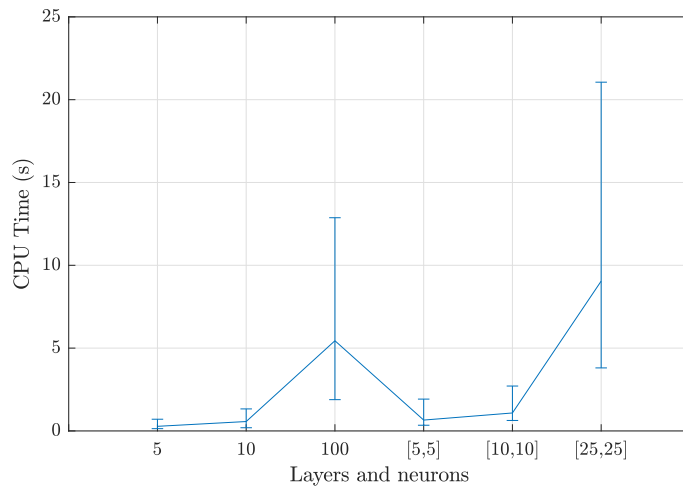


Fig. 2. Block diagram employed in the computation of the float dynamics.

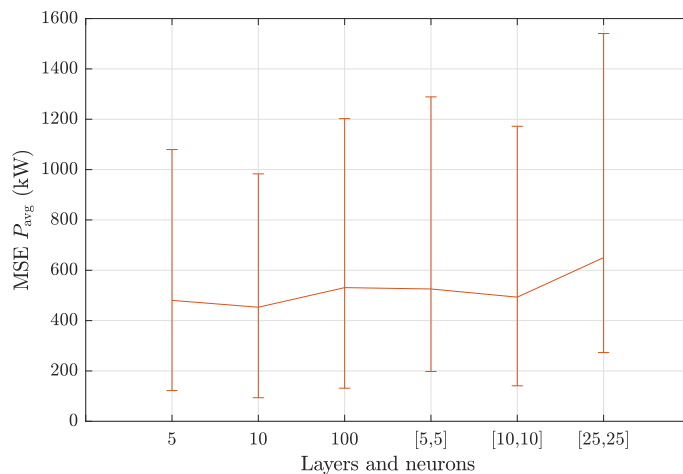


(about 10%) and the remaining 2239 samples for the training set (approximately 90%). For each case, the ANN has been trained using the training samples, and then used to estimate  $P_{avg}$  for the test set. The mean square error between the prediction and the actual mean generated power value has been calculated, as well as the overall computing time required for the ANN implementation described below. Afterwards, the mean and standard deviation of these values have been computed for each network configuration, and plotted in Fig. 3.

From Fig. 3, it is clear that the decision on the size of the ANN should be based on a compromise between performance and accuracy. On the one hand, denser networks result in greater memory requirements and computational cost, as shown in Fig. 3a. In particular, it is interesting to notice that the configuration with two hidden layers with 10 neurons each, which contains a total of 100 connections between the two hidden layers, presents a much lower computational cost than a single layer with 100 neurons, mainly due to implementation reasons. On the other hand, the deeper the network, the greater the number of features that can be matched from the original function; similarly, the greater the number of neurons, the more complex the fitted function shape [16]. An example is the lower mean square error associated with the configurations with 10 neurons as compared with those with 5 in Fig. 3b. Nevertheless, an excessive number of neurons can result in overfitting the input data [27], i.e. fitting the random noise in addition to the underlying relationship, which is highly undesirable since the ANN is expected to generalise the shape of the  $P_{avg}$  and  $\max |z|$  curves. In Fig. 3b, this evidently occurs for a single hidden layer with 100 neurons and two hidden layers with 25 neurons each. Although a single hidden layer seems to perform best, this preliminary study has been carried out on a relatively small dataset, considering only a limited number of sea states.



(a)



(b)

**Fig. 3.** Mean central processing unit (CPU) time (a) and mean square error (MSE) (b) associated with the prediction of the mean generated power for different ANN configurations in terms of hidden layers and neurons for 5 weight initializations and 5 training and test sets. The upper bar corresponds to the sum of the mean value and half the standard deviation, while the lower bar to the minimum value of all cases in order to prevent negative values.

Therefore, it has been preferred to use a configuration with two hidden layers each with 10 neurons in order to represent the possible extra features associated with the additional sea states. Additionally, this results in only a minor increase in computational time. Similar results are obtained from the mapping of the maximum displacement.

A schematic diagram of the feedforward ANN can be seen in Fig. 4. The network presents an input layer with 4 neurons (one for each input variable), two hidden layers with  $m = 10$  and  $n = 10$  neurons each, and an output layer with two output variables. Furthermore, it is possible to see that the input and hidden layers have an additional bias term, which is required to find the intercept of the fitted functions at each stage in the ANN [27]. Each layer  $l$  presents input and output variables, which are expressed as  $\mathbf{x}_l$  and  $\mathbf{y}_l$  respectively in vector notation. The input variables correspond to  $\mathbf{y}_1$ , while the output to  $\mathbf{y}_4$ . The signal between each two matrices is multiplied by weight matrices  $\mathbf{W}_i$ , with  $i = 1, 2, 3$ . The weight matrices for the bias terms are represented as  $\mathbf{b}_i$ .

Given the input data for one training example,  $\mathbf{y}_1$ , it is possible to obtain  $\mathbf{y}_4$ , the ANN estimate for the output by propagating the signal from one layer to the next one. Using this technique, known as forward propagation, the input and output vectors of each layer  $l = 2, 3, 4$  can be computed for each training point in matrix notation, which is convenient from a programming perspective, as follows [27]:

$$\mathbf{x}_l = \mathbf{W}_{l-1}\mathbf{y}_{l-1} + \mathbf{b}_{l-1}, \tag{4}$$

$$\mathbf{y}_l = e_l(\mathbf{x}_l). \tag{5}$$

In (5),  $e_l$  denotes the activation function of the neurons in each layer. Fig. 4 shows that the two hidden layers use the tanh activation function, while the output layer presents a linear activation function. The hyperbolic tangent is a standard smooth, non-linear activation function, which is superior to the sigmoid function, as its output is zero-centred [16]. As described in [16], for a small number of layers, as in this case, tanh is preferred over rectified linear units, which are standard in deep learning. The linear activation function is employed in the output layer in order to return a real value, not bounded within  $\pm 1$  as would be the case if tanh had been used instead.

The mapping between input and output is dictated by the weights of the ANN [16]. Hence, learning can occur by tuning these parameters based on the training data so as to minimize an objective function, which is a measure of the error between actual and predicted output. In order to update the weight matrices, it is necessary to calculate a gradient matrix that indicates the change in the error due to a change in each weight. The gradient matrices are computed by propagating the error signal, or sensitivity,  $\mathbf{s}_l$ , from the output layer to the input layer in a process known as backpropagation [27]:

$$\mathbf{s}_4 = -(\mathbf{y}_{tr} - \mathbf{y}_4) \odot \dot{e}_4(\mathbf{x}_4) \tag{6}$$

$$\mathbf{s}_l = (\mathbf{W}_l^T \mathbf{s}_{l+1}) \odot \dot{e}_l(\mathbf{x}_l), \tag{7}$$

where  $\odot$  indicates the Hadamard, or element-wise, product, and  $\dot{e}_l$  the first derivative of the activation function of each layer.  $\mathbf{y}_{tr}$  indicates the exact output of each training sample, i.e. the variables the ANNs should fit. Therefore,  $\mathbf{y}_{tr} = P_{avg} \max |z|^T$ . The change in the weight matrices is given by [27]:

$$\Delta \mathbf{W}_l = \mathbf{s}_{l+1} \mathbf{y}_l^T, \tag{7}$$

$$\Delta \mathbf{b}_l = \mathbf{y}_l. \tag{8}$$

The equations above are used if the ANNs are trained using one training sample at a time, such as when the simple gradient descent scheme is applied [27]. Nevertheless, batch-mode training, i.e. employing multiple training samples at a time,

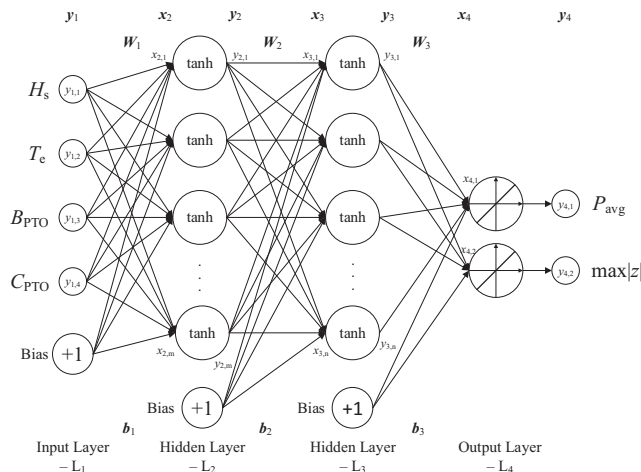


Fig. 4. Schematic diagram of the feedforward ANN for the approximation of the mean generated power or maximum PTO displacement.

is much more efficient. For this reason, the highly efficient Levenberg–Marquardt backpropagation training algorithm has been adopted instead [27]. A detailed explanation of the method, including the necessary extra equations, can be found in [28,27] in matrix notation. The implementation within the Mathworks neural networks toolbox has been used in this work, with the default settings.

It is important to notice that the input variables, i.e.  $H_s$ ,  $T_e$ ,  $B_{PTO}$  and  $C_{PTO}$ , need to be normalized through their mean and standard deviation before being fed to the ANNs for training. Furthermore, the mean power values have also been normalized with respect to the maximum (for positive values) and minimum (for negative values). This has been necessary because the points lying on the  $B_{PTO} = 0$  boundary of the search space presented excessively high negative power values that seriously affected the quality of the function fit.

### 3.2. Multistart optimization

At the start of every new time horizon, the controller should select the PTO damping and stiffness coefficients that will result in maximum energy extraction for the predicted sea state during the horizon, in compliance with the constraint on the PTO displacement. This is clearly a non-linear optimization problem, since both  $P_{avg}$  and  $\max |z|$  are non-linear functions of  $H_s$ ,  $T_e$ ,  $B_{PTO}$  and  $C_{PTO}$ . In addition, the values of the PTO damping and stiffness coefficients must be bounded within sensible values, so that the problem is constrained as well.

By removing the dependence on the significant wave height and wave energy period from functions  $f$  and  $g$  due to space limitations for display purposes, the cost function can be expressed at the start of each new time horizon  $h$  as follows:

$$c(h) = \begin{cases} -f(B_{PTO}, C_{PTO}) & \text{if } |g(B_{PTO}, C_{PTO})| \leq z_{Max} \\ +1 & \text{if } |g(B_{PTO}, C_{PTO})| > z_{Max} \end{cases} \quad (9)$$

subject to:

$$B_{min} \leq B_{PTO} \leq B_{Max}, C_{min} \leq C_{PTO} \leq C_{Max}.$$

The values of the maximum and minimum allowable PTO damping and stiffness coefficients can be derived using accurate, non-linear models during the design stage in order to prevent damage to the generator in the most energetic sea states likely to be encountered, where the buoy velocity and displacement are highest.

Genetic and other nature-inspired algorithms have been extensively used recently for the solution of non-linear optimization problems that present multiple minima, as in this case [29]. Nevertheless, in this work, a strong emphasis is given to performance, since the optimization needs to be repeated at the start of each new time interval. For this reason, it has been preferred to use the Multistart algorithm [30]. This technique consists in generating a number of start points, sampled randomly within the  $B_{PTO}$ ,  $C_{PTO}$  search space. Although convergence is not assured, a large number of starting points greatly increase the chances. A value of 100 starting points has been selected for this reason. From each point, an optimization is run using a non-linear, constrained programming solver. In particular, the Mathworks functions *MultiStart* and *fmincon* have been used respectively. The main advantage of this technique over alternative methods, such as global search, is its simple parallel implementation, which can result in large savings in computational time. For instance, one Multistart optimization using the cost function in (9) takes 8.62 s on a quad-core, i7 computer with 16 GB RAM, whereas a global search takes 29.20 s. A greater number of cores and an implementation in a lower-order language, such as C or Fortran, can result in even greater computational savings.

### 3.3. Algorithm

Fig. 5 shows the algorithm for the ANN-based reactive control of the point absorber described in this article. As aforementioned, a time-averaged approach is used, where new values of  $B_{PTO}$  and  $C_{PTO}$  are selected at the start of every new time horizon  $h$  and applied throughout its duration  $D(h)$ . On the one hand, a longer duration is preferable for the power averaging and sea state statistical analysis so as to produce less noisy training data. On the other hand, a shorter time span can result in faster training. Furthermore, the controller would be able to track changes in the sea state on a smaller time scale, thus moving towards real-time control and possibly higher energy extraction. For these reasons,  $D(h) = 20T_e(h)$  has been chosen in both regular and irregular waves.

As can be seen from Fig. 5, the first step in every time horizon is to predict the significant wave height and energy wave period during the time interval. Different approaches have been proposed for this problem, with example methods being Kalman filters, deterministic sea wave prediction [31], autoregressive models [32], and even ANNs [33]. Although these studies analyse the wave elevation, which is forecast with accuracy only 15 s into the future, it is assumed that similar strategies can be found for the forecast of the statistical wave conditions for one time horizon. For simplicity, in this initial work the actual values for  $H_s$  and  $T_e$  have been used, since the wave traces employed in the simulations are known in advance.  $H_s(h)$  and  $T_e(h)$  are then used to update the count of the number of observations in the current discrete sea state,  $s$ . For this purpose a table,  $\mathbf{N}$ , is employed, with an entry for each discrete sea state with ranges of 1 m and 1 s for each dimension respectively.

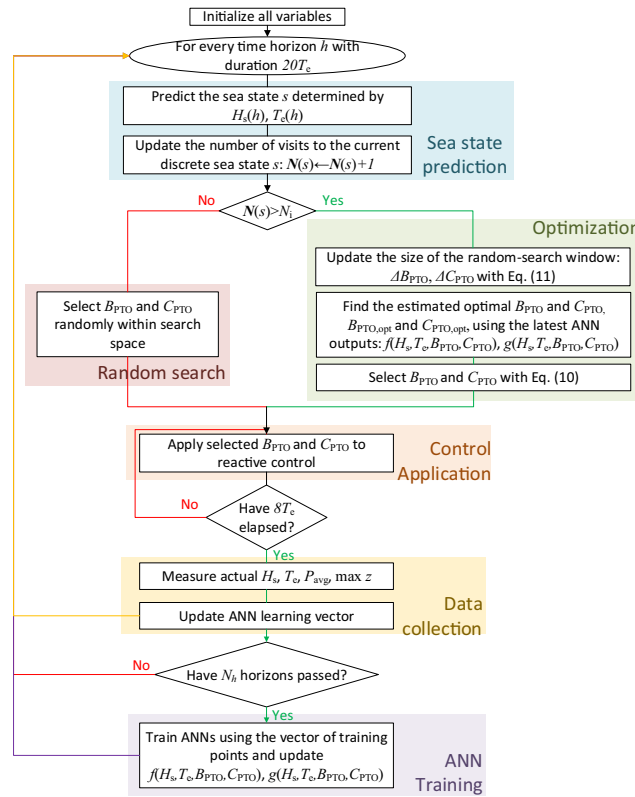


Fig. 5. Flow chart of the ANN-based reactive control of a point absorber.

During the first  $N_i$  visits to each discrete sea state, the values of the PTO damping and stiffness coefficients are selected randomly to ensure initial exploration. Once  $N(s) > N_i$ , the Multistart optimization can be run using the cost function in (9) in order to find the optimal coefficients,  $B_{PTO,opt}$  and  $C_{PTO,opt}$ , for the forecast significant wave height and energy wave period. However, the ANN estimates  $f$  and  $g$  can be very inaccurate initially. For this reason,  $B_{PTO}$  and  $C_{PTO}$  are in fact selected randomly within a region around the optimum that shrinks with the number of data points collected in the sea state:

$$B_{PTO} = B_{PTO,opt} + \Delta B_{PTO}, \quad (10)$$

where

$$\Delta B_{PTO} = (r - 0.5) \cdot \text{range}(B_{PTO}) \cdot 0.9^{N(s)-N_i}, \quad (11)$$

with  $r = [0, 1]$  a random number. The same applies to  $C_{PTO}$ . Upper and lower bounds are used to ensure the chosen values lie within the desired range. As more data points are collected in the optimal region, the accuracy of the ANN fit increases.

Once  $B_{PTO}$  and  $C_{PTO}$  are chosen and applied, measurements are employed to compute the mean absorbed power, maximum PTO displacement and actual  $H_s(h)$  and  $T_e(h)$  during the time interval. These values are in fact calculated using the data only after an initial time of  $8T_e(h)$  within the current horizon  $h$  in order to exclude the initial transient effects. This relatively long time also ensures that the time required for the Multistart optimization does not become an issue. Once the desired values are obtained, they are stored in memory as a data sample so that they can be used for training the ANN.

The ANN is trained every  $N_h = 20$  time horizons, employing 90% of training points. The remaining 10% of the samples is used for validation and hence to check the quality of the fit. Each sample presents  $H_s, T_e, B_{PTO}, C_{PTO}$  as input, and  $P_{avg}$  and  $\max |z|$  as output. The larger the number of training points, the less the risk of overfitting the data and the more accurate the estimates of the ANN. However, this will also cause an increase in training time and, more importantly, it may result in an excessive memory requirement. Therefore, for a practical application, it is expected that the number of training points will be limited to a large number, say  $10^6$ . Care will be needed in order to ensure that a similar number of data points is kept for each discrete sea state when overriding old data with new readings, as well as to explore a broad range of  $B_{PTO}$  and  $C_{PTO}$  values so as to aid the training of the ANN.



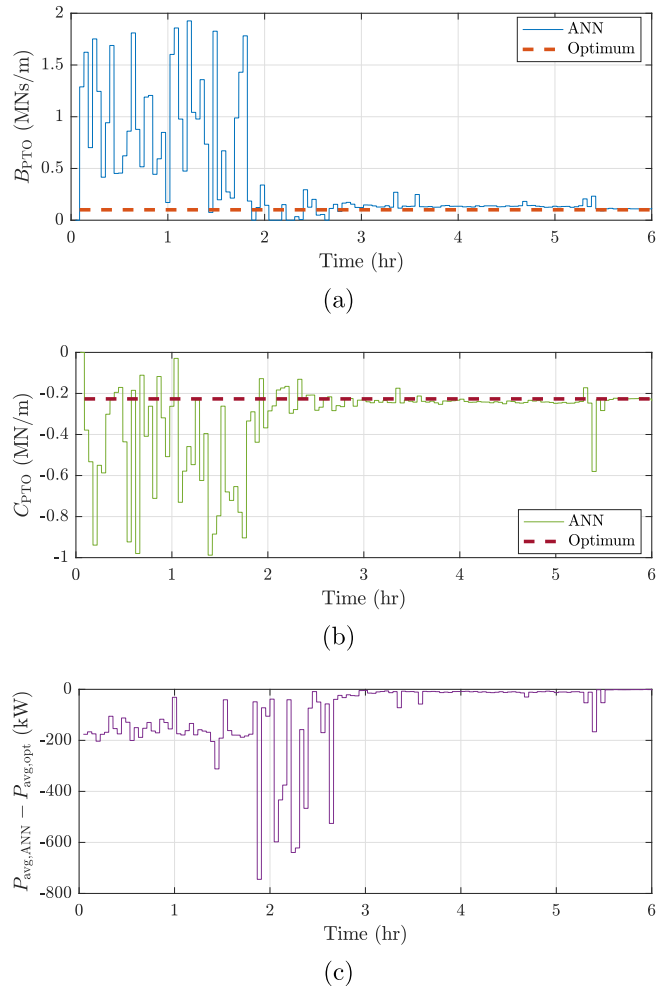


**Fig. 7.** PTO damping (a) and stiffness (b) coefficients obtained from the ANN-based control as compared with the optimal value in regular waves with  $H_s = 2$  m and  $T_e = 8$  s. (c) shows the difference in the corresponding mean generated power.

The learning behaviour of the proposed ANN-based reactive control algorithm in irregular waves is displayed in a compact way in Fig. 8. The figure shows the controller performance for the first wave trace, i.e.  $H_s = 2$  m and  $T_e = 8$  s. In particular, the very first run (when the list of samples is empty at the start) is shown with dotted lines and labelled as “initial”, since learning has just been initialized. The system is simulated in the same wave conditions again *after* the control has been applied for 54 h in the wave traces shown in Table 1. The corresponding performance is shown with continuous lines in Fig. 8 and labelled as “trained”, since learning has completed by then with a large number of samples being available for the training of the ANN. Furthermore, in this case the exploration rate has almost fully decayed, as the discrete sea state has already been experienced for 6 h. Additionally, the optimal value for the PTO coefficients and the corresponding absorbed energy is calculated running a MultiStart optimization of the WEC model in the same wave trace.

## 5. Discussion

### 5.1. Regular waves

As shown in Fig. 7, the ANN-based algorithm learns the optimal PTO damping and stiffness coefficients in regular waves within 4 h after being randomly initialized. In the figures, it is possible to recognize three distinct regions: an initial region where completely random actions are selected ( $\mathbf{N}(s) \leq N_i$ ), a section where random actions are taken around the expected optimum within a shrinking range (until  $0.9^{N(s)-N_i} \rightarrow 0$ ), and a final part where convergence has been reached. Within this last region, it is interesting to notice three random points (after approximately 5.5 h). These are caused by the Multistart algorithm converging towards the wrong local optimum in the corresponding time horizons. This is a possibility that needs to be taken into account when designing the control for an actual device, with its probability decreasing with the number of

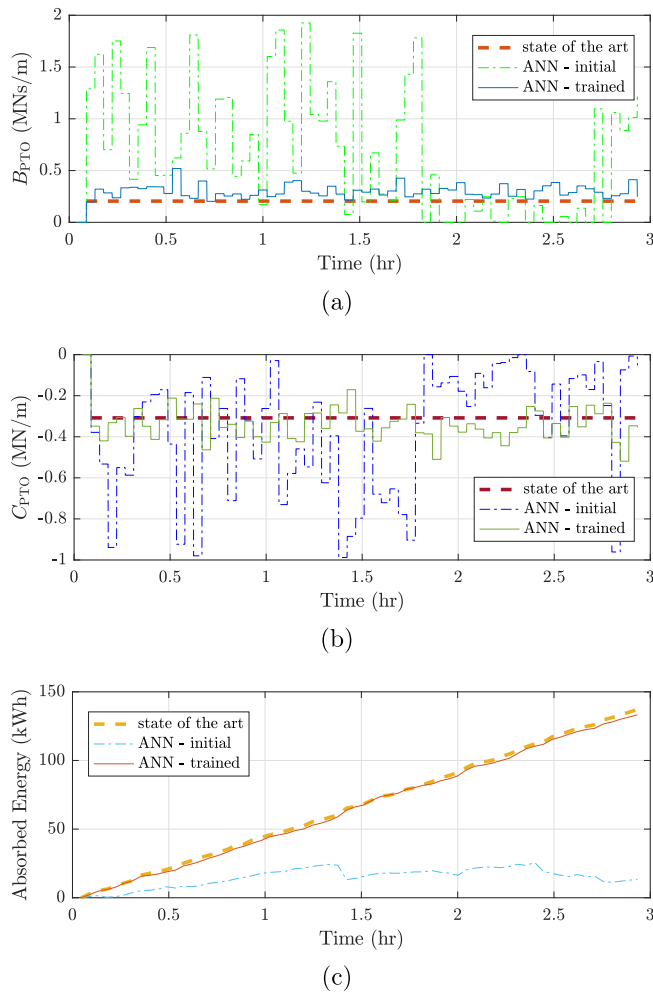


**Fig. 8.** PTO damping (a) and stiffness (b) coefficients adopted by the ANN-based control at the start and after 54-h of training in the wave conditions shown in Table 1 in irregular waves with  $H_s = 2$  m and  $T_e = 8$  s. Additionally, (a) and (b) display the results of state-of-the-art reactive control. The corresponding curves for the absorbed energy are plotted in (c).

starting points. Nevertheless, the low computational cost means this optimization method is still preferred over global search or genetic algorithms. Oddly, the three random points also provide the ANNs with the missing training points for perfect convergence to the optimal PTO coefficients.

It should be noted that the ANN-based algorithm presents faster learning than reinforcement learning, which requires approximately 6 h in regular waves with resistive control and 8 h with reactive control in [14,15], respectively.

## 5.2. Irregular waves

The convergence of the algorithm to the optimal PTO coefficients in irregular waves is shown by the "trained" lines in Fig. 8. Oscillations in the values obtained with the ANN-based control are due to changes in wave conditions over the smaller time scale of  $20T_e$ . The energy absorption is almost identical to state-of-the-art reactive control applied using the optimal coefficients for the WEC model in this wave trace.

In this case, the comparison in learning performance between reinforcement learning and ANNs is harder to understand. At first sight, 54 h may seem like a very long learning time. However, this corresponds to 6 h of learning time per discrete sea state, which is less than the 10 h required by reinforcement learning in a single sea state of irregular waves for resistive control in [14]. Once a sufficient number of points is obtained, the ANN can generalise the information to unseen sea states, thus further reducing the learning time as compared with reinforcement learning with discrete states. In addition, the convergence time should be assessed in the context of the lifetime of a WEC, which is expected to be 20–25 years long [25].

In this work, discrete sea states have been analysed, each lasting 3 h due to practical issues with the code implementation. In reality, the energy content in waves changes uniformly in time (hence, not through discrete sea states), with the duration

of a typical sea state being 0.5 to 6 h [26]. Since  $P_{\text{avg}}$  and  $\max |z|$  can be considered to be purely dependent on the values of  $B_{\text{PTO}}$ ,  $C_{\text{PTO}}$ ,  $H_s$  and  $T_e$  in the *current* time interval, the samples of the ANN are independent of past data. Therefore, the algorithm can be safely applied to realistic, continuously varying wave conditions. In fact, the quality of the mapping provided by the ANN is expected to improve in continuously varying sea states, which result in a broader range of samples [27]. Furthermore, under realistic wave conditions, the ANN-based reactive control is expected to result in higher energy absorption than state-of-the-art reactive control, since the latter uses a look-up table with discrete sea states, thus being less responsive to changes in wave energy over a shorter time scale. Additionally, the ANN-based method can adapt to changes in the device dynamics with time, e.g. due to marine growth.

### 5.3. Practical considerations

Although ANNs are a supervised learning strategy, they are employed here in an approach reminiscent of reinforcement learning, which is unsupervised, and that entails exploration. This may result in damage to and even failure of the device if explorative negative actions are selected at the wrong time, e.g. a high PTO stiffness coefficient with low damping in highly energetic waves. Strategies that rely on explorations suffer from this problem, but the ANN-based control is more affected than reinforcement learning because:

- reinforcement learning [15] makes a step change in the PTO coefficients at the start of each interval. Hence, it is difficult to encounter highly negative situations, since the algorithm corrects the PTO coefficients as soon as it starts receiving negative feedback on the actions it has selected in that particular sea state. Conversely, the proposed ANN-based method is able to explore the whole search space during the first observations of a particular discrete sea state.
- the quality of the mapping produced by the ANN is improved for a wider range of samples. Hence, in order to improve the training process, the algorithm is incentivized to explore most combinations of the PTO coefficients in each sea state.

In order to prevent failure or damage to the WEC, two practical possibilities should be investigated:

- initializing the ANN with samples pre-generated using accurate, non-linear models of the WEC. In particular, simulations should be run using extreme values of the PTO coefficients so that once the algorithm is applied on the real-device, the Multi-Start optimization should home in onto the optimal conditions rather than risk selecting extreme control settings.
- an alternative approach consists in initially applying state-of-the-art reactive control with the look-up table approach and slowly changing the PTO coefficients in each sea state. The collected data will be then employed for the training of the ANN, and then the proposed algorithm will be applied. This process is designed to remove the exploration stage from the presented scheme, focusing only on the supervised nature of ANN algorithms.

At the moment, exact knowledge of the values of  $H_s$  and  $T_e$  during the following time horizon is assumed. In practice, errors will be associated with the estimation method [31–33]. Nevertheless, including information on the expected future wave excitation is a fundamental tool for the control of WECs in order to try to achieve optimal performance [5]. This is a further improvement over the reinforcement learning algorithm proposed in [15], since the study assumed the wave height and period to be identical between neighbouring horizons.

As compared with reinforcement learning, the selection of the control action with the proposed method requires greater computational power. Nevertheless, an on-line implementation is completely feasible with modern hardware and parallel computing. As described in Section 3.3, the control strategy consists in two main stages. On the one hand, the weight of the ANNs are updated every 20 algorithm steps, using all training points (at most, say,  $10^6$ ). This process occurs off-line, with the older weights not being overwritten on the memory until the new ones are ready, so that computing time is not an issue. On the other hand, at every time step, a new training point is collected (minimal computation effort), and a new action is selected through the Multistart optimization. This process is speeded up through parallel processing, and possibly an implementation in a low-order computational language, e.g. C. As described in Section 3.2, one optimization using the current simulation in Matlab and a quad-core i7 computer with 16 GB RAM takes less than 9 s. This period is less than 10% of the minimal expected time horizon duration, namely 100 s for a 5-s wave energy period, which is the smallest encountered in typical sea states [26]. Hence, computation efficiency is not critical in this case, since the rate of change of the plant is much slower than that of the control algorithm.

Real-time strategies are more efficient than time-averaged methods for the control of WECs [5]. Hence, although machine learning schemes are interesting due to their model-free approach of the WEC control problem, they will need to be applied in real-time in order to compete with model-predictive control. The application of real-time system identification with ANNs to real-time strategies, such as model predictive control, will be investigated in the future.

## 6. Conclusion

In this article, an on-line, model-free strategy has been developed for the reactive control of WECs using ANNs. The aim is to maximise energy absorption, whilst limiting the PTO displacement to prevent failure in energetic sea conditions. A simple

model of a point absorber has been employed to analyse the behaviour of the algorithm. Firstly, regular waves show that the strategy learns rapidly the optimal PTO damping and stiffness coefficients because of their periodicity. A longer convergence time is necessary in irregular waves, since the ANNs require a greater number of training samples in order to learn the mapping between the mean absorbed power and PTO displacement, and the significant wave height, wave energy period, and the PTO damping and stiffness coefficients. Nevertheless, this ensures the scheme can recognize variations in the wave conditions on a shorter time scale than state-of-the-art reactive control, which uses discrete sea states. Furthermore, implementation on a full-scale WEC is simple, as the technique is independent of models of the machine dynamics. More importantly, this method is able to treat changes in the device response as the structure is affected by marine biofouling.

## Acknowledgment

The Industrial Doctoral Training Centre for Offshore Renewable Energy is a partnership of the universities of Edinburgh, Exeter and Strathclyde. This work was supported partly by the Energy Technologies Institute and the Research Councils Energy Programme (grant EP/J500847/), and partly by the Engineering and Physical Sciences Research Council (grant EP/J500847/1). Additionally, the first author's Eng.D. project is sponsored by Wave Energy Scotland.

Wave Energy Scotland is taking an innovative approach to supporting the development of wave energy technology by managing the most extensive technology programme of its kind in the sector, concentrating on key areas which have been identified as having the most potential impact on long term levelised cost of energy and improved commercial viability.

## References

- [1] K. Gunn, C. Stock-Williams, Quantifying the Potential Global Market for Wave Power, in: Proceedings of the 4th International Conference on Ocean Engineering (ICOE 2012) (2012) 1–7.
- [2] A.F.D.O. Falcão, Wave energy utilization: a review of the technologies, *Renew. Sustain. Energy Rev.* 14 (3) (2010) 899–918, <http://dx.doi.org/10.1016/j.rser.2009.11.003>.
- [3] A.J. Nambiar, D.I.M. Forehand, M.M. Kramer, R.H. Hansen, D.M. Ingram, Effects of hydrodynamic interactions and control within a point absorber array on electrical output, *Int. J. Marine Energy* 9 (2015) 20–40, <http://dx.doi.org/10.1016/j.ijome.2014.11.002>.
- [4] S.H. Salter, J.R.M. Taylor, N.J. Caldwell, Power conversion mechanisms for wave energy, *Proc. I MECH E Part M* 216 (1) (2002) 1–27, <http://dx.doi.org/10.1243/147509002320382112>.
- [5] J.V. Ringwood, G. Bacelli, F. Fusco, Energy-maximizing control of wave-energy converters: the development of control system technology to optimize their operation, *IEEE Control Syst. Mag.* 34 (5) (2014) 30–55.
- [6] K. Budal, J. Falnes, Optimum operation of wave power converter, *Marine Sci. Commun.* 3 (2) (1977) 133–150.
- [7] A. Babarit, A.H. Clément, Optimal latching control of a wave energy device in regular and irregular waves, *Appl. Ocean Res.* 28 (2) (2006) 77–91, <http://dx.doi.org/10.1016/j.apor.2006.05.002>.
- [8] J. Hals, J. Falnes, T. Moan, Constrained optimal control of a heaving buoy wave-energy converter, *J. Offshore Mech. Arct. Eng.* 133 (1) (2011) 011401, <http://dx.doi.org/10.1115/1.4001431>.
- [9] T.K.A. Brekken, On model predictive control for a point absorber wave energy converter, *Proc. IEEE Trondheim PowerTech* (2011) 1–8, <http://dx.doi.org/10.1109/PTC.2011.6019367>.
- [10] F. Fusco, J.V. Ringwood, A simple and effective real-time controller for wave energy converters, *IEEE Trans. Sustainable Energy* 4 (1) (2013) 21–30, <http://dx.doi.org/10.1109/TSTE.2012.2196717>.
- [11] K.U. Amann, M.E. Magaña, S. Member, O. Sawodny, Model predictive control of a nonlinear 2-body point absorber wave energy converter with estimated state feedback, *IEEE Trans. Sustainable Energy* 6 (2) (2015) 336–345.
- [12] D. Oetinger, M.E. Magaña, S. Member, O. Sawodny, Decentralized model predictive control for wave energy converter arrays, *IEEE Trans. Sustainable Energy* 5 (4) (2014) 1099–1107.
- [13] O. Sawodny, D. Oetinger, M.E. Magaña, Centralised model predictive controller design for wave energy converter arrays, *IET Renew. Power Gener.* 9 (2) (2015) 142–153, <http://dx.doi.org/10.1049/iet-rpg.2013.0300>.
- [14] E. Anderlini, D.I.M. Forehand, P. Stansell, Q. Xiao, M. Abusara, Control of a point absorber using reinforcement learning, *Trans. Sustainable Energy* 7 (4) (2016) 1681–1690.
- [15] E. Anderlini, D.I.M. Forehand, E. Bannon, M. Abusara, Constraints implementation in the application of reinforcement learning to the reactive control of a point absorber, in: Proceedings of the ASME International Conference on Ocean, Offshore and Arctic Engineering, Trondheim (2017) June 25–30.
- [16] Y. LeCun, Y. Bengio, G. Hinton, Deep learning, *Nature* 521 (7553) (2015) 436–444, <http://dx.doi.org/10.1038/nature14539>, arXiv:arXiv:1312.6184v5.
- [17] D. Valério, M.J.G.C. Mendes, P. Beirão, J. Sá da Costa, Identification and control of the AWS using neural network models, *Appl. Ocean Res.* 30 (3) (2008) 178–188, <http://dx.doi.org/10.1016/j.apor.2008.11.002>.
- [18] S. Giorgi, J. Davidson, J.V. Ringwood, Identification of wave energy device models from numerical wave tank data Part 2: data-based model determination, *IEEE Trans. Sustainable Energy* 7 (3) (2016) 1020–1027, <http://dx.doi.org/10.1109/TSTE.2016.2515500>.
- [19] E. Tedeschi, M. Carraro, M. Molinas, P. Mattavelli, Effect of control strategies and power take-off efficiency on the power capture from sea waves, *IEEE Trans. Energy Convers.* 26 (4) (2011) 1088–1098, <http://dx.doi.org/10.1109/TEC.2011.2164798>.
- [20] L. Castellini, M.D. Andrea, N. Borgarelli, Analysis and Design of a Reciprocating Linear Generator for a PTO, in: International Symposium on Power Electronics, Electrical Drives, Automation and Motion Analysis, 2014, pp. 1373–1379.
- [21] C. Wei, Z. Zhang, W. Qiao, L. Qu, An Adaptive Network-Based Reinforcement Learning Method for MPPT Control of PMSG Wind Energy Conversion Systems, *IEEE Transactions on Power Electronics* 8993 (c) (2016) 1–1. doi:10.1109/TPEL.2016.2514370.
- [22] J.N. Newman, *Marine Hydrodynamics*, MIT Press, 1977.
- [23] W.E. Cummins, The impulse response function and ship motions, *Schiffstechnik* 47 (9) (1962) 101–109.
- [24] D. Forehand, A.E. Kiprakis, A. Nambiar, R. Wallace, A bi-directional wave-to-wire model of an array of wave energy converters, *IEEE Trans. Sustainable Energy* 7 (1) (2016) 118–128, <http://dx.doi.org/10.1109/TSTE.2015.2476960>.
- [25] J. Cruz, *OceanWave Energy*, Springer-Verlag, 2008.
- [26] L.H. Holthuijsen, *Waves in Oceanic and Coastal Waters*, Cambridge University Press, 2007.
- [27] M.T. Hagan, H.B. Demuth, M.H. Beale, O. De Jesús, *Neural Network Design*, second ed., PWS Publishing, 1996.
- [28] M.T. Hagan, M.B. Menhaj, Training feedforward networks with the Marquardt algorithm, *IEEE Trans. Neural Networks* 5 (6) (1994) 989–993, <http://dx.doi.org/10.1109/72.329697>.
- [29] J.S. Arora, Introduction to Optimum Design, third ed., Academic Press, 2012, <http://dx.doi.org/10.1016/B978-0-12-381375-6.00009-7>, arXiv:arXiv:1011.1669v3.

- [30] Z. Ugray, L. Lasdon, J. Plummer, F. Glover, Scatter search and local NLP solvers: a multistart framework for global optimization, *Information Systems* 19 (May) (2006) 328–340, <http://dx.doi.org/10.1287/ijoc.1060.0175>.
- [31] G. Li, G. Weiss, M. Mueller, S. Townley, M.R. Belmont, Wave energy converter control by wave prediction and dynamic programming, *Renewable Energy* 48 (2012) 392–403.
- [32] F. Fusco, J.V. Ringwood, Short-term wave forecasting with ar models in real-time optimal control of wave energy converters, *IEEE Int. Symp. Ind. Electron.* (2010) 2475–2480, <http://dx.doi.org/10.1109/ISIE.2010.5637714>.
- [33] H.E. Shoori J., B. Ling, B.A. Batten, Use of artificial neural networks for real-time prediction of heave displacement in ocean buoys, in: 3rd International Conference on Renewable Energy Research and Applications, ICRERA 2014 (2015) 907–912 doi: 10.1109/ICRERA.2014.7016517.
- [34] G.F. Franklin, J.D. Powell, A. Emami-Naeini, *Feedback Control of Dynamic Systems*, 6th ed., Pearson, 2008.
- [35] J. Falnes, *Ocean waves and Oscillating systems*, paperback Edition., Cambridge University Press, 2005, [http://dx.doi.org/10.1016/S0029-8018\(02\)00070-7](http://dx.doi.org/10.1016/S0029-8018(02)00070-7).